Effect of Aeromonas hydrophila infected on metabolomic response and gut microbial 16S rRna of *Charybdis japonica*

Mingming Han[2], Chenxi Zhu[1], Zakaria Zuraini[2], Tianheng Gao[3], Ying Yang[1], Tongqing Zhang[1], Feng Ji[4], Qichen Jiang[1*]

[1] *Freshwater Fisheries Research Institute of Jiangsu Province. 79 Chating East Street, Nanjing 210017, China*

[2] *Biology Program, School of Distance Education, Universiti Sains Malaysia, 11800 Minden, Penang, Malaysia*

[3] *Institute of Marine Biology, College of Oceanography, Hohai University, China*

[4] *Jiangsu Key Laboratory for Molecular and Medical Biotechnology, College of Life Sciences, Nanjing Normal University, Nanjing, 210023, China*

* Corresponding author e-mail: qichenjiang@live.cn;

Abstract

The innate immune response of *Charybdis japonica* treated with *Aeromonas hydrophila* was explored using bioinformatics. Metabolomics data were integrated with a gut microbial 16S rRNA dataset, together with information on corresponding enzyme activity. The results of the study showed that after being infected with *A. hydrophila*, some beneficial genera of bacteria in the gut of *C. japonica*, such as Photobacterium, Rhodobacter, Polaribacter, Psychrilyobacter, Mesoflavibacter, Fusibacter and Phormidium, could directly inhibit Vibrio or produce extracellular polysaccharides with highly effective antibacterial properties. The intestinal probiotics

of *C. japonica* such as Mesoflavibacter have a mutually reinforcing relationship with Phaeobacter, Colwellia, Bacillus, Psychrobacter and Cohaesibacter. Conditional pathogenic bacteria in the gut of healthy crabs may also have such a symbiotic relationship with intestinal probiotics, promoting their growth and reproduction. For example, Phormidium has a mutualistic relationship with *Aeromonas* and Azopira. Metabolites in the gut of *C. japonica* infected with *A. hydrophila*, including beta-alanine metabolism, nitrogen metabolism, inositol phosphate metabolism, galactose metabolism, histidine metabolism, ascorbate and arginine and proline metabolism were increased, with alanine metabolism being the most abundant. The activity of metabolite related enzymes such as lipid peroxidase, phenoloxidase, superoxide dismutase, nitric oxide synthase, glutathione transferase and mid-glutathione decreased and NO levels also decreased. The positive correlation with the probiotic flora suggests that metabolites increase with bacterial abundance and that microbial metabolites or co-metabolites can, in turn, achieve many pleiotropic effects to resist invasion by *A. hydrophila*. These results may contribute to further research in the resistance of *C. japonica* to invading pathogens.

Importance

With the rapid development of the *C. japonica* farming industry, investors, in pursuit of economic benefits, have encountered problems such as frequent outbreaks of various diseases, resulting in high mortality and huge economic losses. The open water circulation system can give rise to several crab bacterial diseases. Among these, *A. hydrophila* is a pathogenic bacterium affecting fish and crustaceans, which leads to

huge economic losses. Our results suggest that metabolites increased with the abundance of bacteria. It is possible that the autoimmune system and the entry of *A. hydrophila* into the intestinal tissues of *C. japonica* react immunologically and that the organism is producing certain metabolites which may be metabolised by various bacteria and absorbed into the circulation. In addition, some of these metabolites are modified or bound in the hepatopancreas to produce microbiota-host co-metabolites. These microbial metabolites or co-metabolites can resist invasion by *A. hydrophila*.

Key words: Metabolome, innate immunity, 16S rRNA, *Charybdis japonica*, *Aeromonas hydrophila*

1. Introduction

Charybdis japonica is found as an important edible species in the intertidal zone along the west coast of the Pacific Ocean, including China, Japan and Malaysia. The habitat of *C. japonica* is frequently affected by pathogenic bacteria of the Vibrio family(1). *A. hydrophila* belongs to the family Vibrionaceae and the genus *Aeromonas*, which is a group of thermophilic hydrophilic *Aeromonas*. It is ubiquitous in nature, is pathogenic to aquatic animals (2) and can cause septicaemia in various aquatic animals, bringing economic losses to the freshwater aquaculture industry, thus attracting the attention of fisheries, veterinary and medical researchers (3). In aquaculture, a complex micro-ecosystem exists in the gut that functions for digestion, nutrient absorption and disease resistance (4). The gut-associated microbiota plays a unique role in host gut development, immune response, disease resistance and

67 homeostasis. Beneficial strains of bacteria and beneficial metabolites have been
68 introduced into the host gut with significant results(5). The microbial composition of
69 the gut of crustaceans has a significant impact on animal health, growth and survival.
70 Factors such as the internal structure of shrimps and crabs, host conditions, diet,
71 climate change, living environment, and bacterial or viral infections can all affect the
72 gut flora of aquatic animals(5). This experiment is designed to understand the role of
73 bacteria in the gut of crabs, firstly by understanding the composition of host gut
74 bacterial flora. Secondly, it is important to discover the changes in the composition of
75 the gut bacterial flora after infection with the bacteria.
76
77 For crabs, the microbial diversity of crab carapace, gut and haemolymph fluid was
78 studied by using 16S rRNA gene analysis, cloning and sequencing (6), and various
79 potential pathogens were examined, such as *Alternaria alternata*, *Bacillus*,
80 *Escherichia coli*, photobacterium subspecies and *Vibrio harveyi*. They have greatly
81 expanded our view of the microbial life associated with marine invertebrates, such as
82 microbial community composition, functional potential and metabolic activity (7). In
83 recent years, the diversity of gut microbes in a variety of aquatic animals has been
84 studied based on 16S rRNA genes, and the gut microbial diversity of shrimp has been
85 investigated by molecular isolation (8). A comparison of the gut microbiota of healthy
86 and diseased crabs revealed that the relative abundance of bacteria in healthy crabs
87 was higher than in diseased crabs (9). *Scylla paramamosain* was infected with *Vibrio*
88 *vulnificus* and strains were screened for antagonistic activity against *Vibrio*

parahaemolyticus using an agar spot assay. The antagonistic strains were then identified by 16S rRNA gene sequence analysis (10). The 16SrRNA method has been important in the analysis of crab infection with bacteria.

Metabolomics is a method of histological measurement and an important tool in histology. Metabolomics methods allow the unbiased analysis of the composition of all detectable metabolites, and thus, rapid quantitative detection of stress responses(11). Metabolomics has been shown to provide in-depth research data in crab diet, climate change, living environment, physiology and pathology and biochemistry (12). *A. hydrophila* infects aquatic animals through incidental bruises on the body. Metabolomics is also an important tool to study the innate immunity of *C. japonica*.

This experiment first studied the innate immunity of *C. japonica* infected with *A. hydrophila*. The aims of the study were 1) to examine the composition of the intestinal bacterial flora by the 16S rRNA sequencing technique, discover the changes in the composition of the intestinal bacterial flora after infection with *A. hydrophila*; 2) to find differential metabolites and the function of these metabolites through metabolome sequencing; 3) to investigate and understand the relationship between metabolites and gut microbes by integrating metabolomics data with gut microbial 16S rRNA datasets using bioinformatics tools; 4) to analyse relevant enzyme activities that affect metabolites.

2. Experimental methods

2.1. Experimental materials

Samples of *C. japonica* were collected from the South China Sea. The crabs weighed 81 ± 3.4 g and body length and width were 8 ± 1.7 cm and 6 ± 1.6 cm, respectively. One hundred and twenty *C. japonica* were divided equally into six aquariums with identical nets and PVC pipes to act as a shelter for the animals and prevent cannibalism. They were fed (9812; Shanghai Harmony Feed Co., Ltd., China) at 8:00 and 18:00 daily with the equivalent of 5% of the body weight of a pair of *C. japonica*. The crabs were exposed to seawater using an artificial sea salt cycle (salinity 28 psu), with water temperature controlled at 25 ± 1°C, pH 8.0 ± 0.2, a dissolved oxygen concentration of 5.0 mg L^{-1} and a 12 h light/dark cycle.

After 2 weeks of acclimation, water quality was maintained at the same level as in the acclimation period. Animals were not fed commercial feed for 24 hours before the trial. Sixty animals were removed from three aquaria for bacterial infection experiments, and 10^5 CFU/L of *A. hydrophila* was injected into the fourth leg. An equal amount of saline was injected into the fourth leg of 60 animals in the remaining three aquaria, and samples were collected 24 hours later. Intestinal and hepatopancreas tissue was collected with sterile scissors and forceps after anaesthetizing the crabs on ice. All intestinal tissues and hepatopancreas were then rapidly frozen in liquid nitrogen and stored at −80°C for subsequent experiments. To avoid errors due to individual differences, composite samples were prepared by

133 mixing equal amounts of each group of intestinal tissues and then aliquoting them into
134 two samples. Some samples were assayed for relevant immune genes and enzymes.
135 The *A. hydrophila* for this study was provided by Shanghai Ocean University. *A.*
136 *hydrophila* freezing tubes were removed from storage at −80°C and quickly
137 transferred to a water bath at 37°C to rapidly dissolve the bacterial freezing tract
138 solution. After observation, to ensure that *A. hydrophila* was free of contamination,
139 LB solid plates were recoated with bacteria and incubated in a constant temperature
140 incubator at 28°C for 20 h. The *A. hydrophila* were grown to log phase and diluted to
141 10^5 cfu/L by the McElloby method.
142
143 2.2. DNA extraction and PCR amplification
144 The mixed intestinal tissues were subjected to total DNA extraction using an
145 E.Z.N.A.® soil kit (Omega Bio-Tek, Norcross, GA, USA). DNA concentration and
146 purity were assayed using NanoDrop2000. DNA extraction quality was checked by 1%
147 agarose gel electrophoresis. PCR amplification of V3-V4 was performed using
148 primers 338F (5′-ACTCCTACGGGAGGCAGCAG-3′) and 806R (5′-
149 GGACTACHVGGGTWTCTAAT-3′). PCR products were recovered using a 2%
150 agarose gel, and purified using the AxyPrep DNA Gel Extraction Kit (Axygen
151 Biosciences, Union City, CA, USA), eluted in Tris-HCl and detected by 2% agarose
152 electrophoresis. Quantification was carried out by using QuantiFluor™-ST (Promega,
153 USA).
154

155 2.3. Illumina Miseq sequencing

156 The purified amplicons were constructed into PE 2*300 libraries according to the
157 Illumina MiSeq platform (Illumina, San Diego, USA) standard operating protocols.
158 The raw sequence fastq files were imported into a file format ready for subsequent
159 processing by QIIME2. The QIIME2 dada2 plug-in was then applied for quality
160 control, pruning, denoising, splicing and removal of chimaeras to obtain the final
161 table of characteristic sequences. Next, the ASV representative sequences were
162 compared to the 99% similarity GREENGENES database (the database was trimmed
163 to the V3V4 region based on the 338F/806R primer pair) to obtain a taxonomic
164 information table for the species, removing all contaminating mitochondria. Methods
165 such as ANCOM, ANOVA, Kruskal Wallis, igraph, LEfSe and DEseq2 were used to
166 identify groupings. The R package "mixOmics" was used for bacteria with differences
167 in abundance between samples, and partial least squares discriminant analysis (PLS-
168 DA) was used as a supervised discriminant analysis statistical method to reveal the
169 relationship between microbial communities and sample classes and to enable the
170 prediction of sample classes based on the relative abundance of the main microbial
171 species in the sample. We also used co-occurrence analysis to calculate Spearman's
172 rank correlation coefficients, which were used to understand associations between
173 species. In addition, PICRUSt software was used to predict the likely functional
174 composition of the microbial community. Unless specifically noted, the parameters
175 used in the above analyses are the default settings.

176

177 2.4. Metabolite extraction

178 Intestinal tissue (100 mg) was placed into a 5 mL tube (reduced by equal proportions
179 if the sample size was insufficient) and mixed thoroughly for 1 min with 500 μL
180 ddH_2O at 4 °C. Methanol (1 mL, −20 °C) and heptadecanoic acid (60 μL 0.2 mg/mL)
181 were added, shaken in a Vortex for 30 s, sonicated for 10 min at room temperature,
182 left on ice for 30 min and centrifuged at 12 000 *g* for 10 min at 4 °C. The supernatant
183 was transferred to a new 1.5 mL centrifuge tube and the sample was concentrated by
184 vacuum centrifugal concentrator. Methoxy solution (60 μL) was added and shaken in
185 a Vortex for 30 s. The reaction was carried out at 37 ℃ for 2 h. Finally, 60 μL of
186 reagent (containing 1% trimethylchlorosilane) was added and the reaction was carried
187 out at 37 ℃ for 90 min and centrifuged at 10 000 g for 10 min at 4 ℃. The reaction
188 was carried out at 37 °C for 90 min and centrifuged at 10 000 g for 10 min at 4 °C.
189 The supernatant was added to a vial and part was used in quality control to correct for
190 deviations in the results of mixed samples and errors caused by the analytical
191 instrument, the remaining sample was used for GC-MS.

192

193 2.5. On-board testing

194 Gas chromatography was performed on an HP-5MS capillary column (5% benzene/95%
195 methyl polysiloxane 30 m × 250 μm i.d., 0.25 μm film thickness, Agilent J & W
196 Scientific, Folsom, CA, USA) with a constant flow of helium at 1 mL/min. The 1 μL
197 sample was injected through an autosampler at a 20:1 split ratio. The injection
198 temperature was 280 °C, set to 150 °C for the interface and adjusted to 230 °C for the

ion source. Mass spectrometry was performed using a full scan method with a range of 35 to 750 (m/z)

2.6. Data pre-processing steps

The data obtained were subjected to GC-MS metabolomics assays for bioinformatics analysis. The raw data were converted into netCDF format (xcms input file format) by an Agilent MSD ChemStation workstation for peak identification, peak filtration and peak alignment. A data matrix including mass to charge ratio (m/z) and retention time and peak area (intensity) was obtained. The metabolites were annotated in conjunction with the AMDIS program using the National Institute of Standards and Technology (NIST) commercial database and the Wiley Registry Metabolome database. The metabolite alkane retention indices were provided according to The Golm Metabolome Database (GMD) (http://gmd.mpimp-golm.mpg.de/) and used for further substance characterisation. The detailed data results, which are normalised internally to allow for comparison between different quantities of data.

2.7. Measuring the activity of hepatopancreas-related enzymes

Hepatopancreas (100 mg) was homogenised with nine times the volume of physiological saline solution by weight to make a 10% tissue homogenate. The homogenate was centrifuged at 2500 rpm at 4°C for 10 min and the supernatant was placed on ice for assays. The activities of hepatopancreas-related enzymes were measured using kits from the Nanjing Jiancheng Company. Protein concentrations

were determined by the Folin-phenol method and hexokinase activity was determined by a colourimetric method coupled to 6-phosphoglucose dehydrogenase. Superoxide dismutase (SOD), phosphofructokinase (PFK), pyruvate kinase (PK), nitric oxide synthase (i-NOS), lipid peroxidase (LPO), phenoloxidase (POX), glutathione transferase (GST), glutathione (GSH), glutathione peroxidase (GPX) and glutathione reductase (GR) were tested according to the manufacturer's instructions. GPX was measured at 412 nm absorbance, GSH at 405 nm absorbance and GST at 412 nm absorbance. GST was measured by absorbance at 340 nm using 1-chloro-2,4-dinitrobenzene as the substrate. The absorbance of each tube was measured at 550 nm with a 1 cm optical diameter of 0.4 mm inner diameter and blanked with distilled water to detect nitric oxide (NO).

3. Results

3.1. C. japonica 16S rRNA sequencing data

After removing low-quality reads, a total of 577,767 valid reads were obtained from the 12 samples. The highest number of valid reads in all the samples of AH1 was 58,952 (Figure 2A) and the lowest number of valid reads in all the samples of CK was 32,453. The mean value of valid reads was 48,147.25. The highest number of optimized non-chimeric sequences in all the samples of AH1 was 42540 and the lowest number of optimized non-chimeric sequences in CK6 was 14226. The abundance of microorganisms in the gut of *C. japonica* can be assigned to the most classifiable taxa such as phylum, phylum, order, family and genus. Of the total 48

243 samples from the three groups, 99% of the phylotypes belonged to only four core
244 phyla: Proteobacteria (0.92%), Tenericutes (5.21%), Fusobacteria (2.61%) and
245 Bacteroidetes (0.73%; Figure 2).
246
247 3.2. Annotation and assessment of species
248 The distribution of the four dominant phyla was relatively similar across samples in *C.*
249 *japonica* infected with *A. hydrophila*, but with different trends in abundance and
250 variation. Figure 2 shows that there were 84 CK endemic species, 77 AH endemic
251 species and 110 shared species. Alpha diversity indices were analysed (Figure 2B) for
252 both richness and evenness of species composition in the 12 samples. Figure 2C
253 shows that there were only 10 samples with a Shannon index of 2 or more for AH and
254 CK.
255
256 3.3. Species-specific phylogenetic analysis
257 The phylogenetic evolutionary tree in Figure 3A for Polaribacter and Mesoflavibacter
258 shows that the relative abundance of AH of Polaribacter after infection with *A.*
259 *hydrophila* was 0.442326. The relative abundance of AH of Mesoflavibacter after
260 infection with *A. hydrophila* was 0.216081. The relative abundance of Photobacterium
261 in Firmicutes and Proteobacteria in the phylogenetic evolutionary tree was 0.421645
262 after infection with *A. hydrophila* and 0.288675 after infection with *Rhodobacter*
263 *hydrophila*. In the phylogenetic tree, Psychroserpens in Fusobacteria had a higher AH
264 relative abundance of 0.290992 after infection with *A. hydrophila*, and Fusibacter in

Firmicutes had a higher AH relative abundance of 0.288675 after infection with *A. hydrophila*. The relative abundance of Phormidium in Cyanobacteria was 0.288675 after infection with *A. hydrophila*.

3.4 Species interaction network analysis

As can be seen in Figure 3B, Rhodobacter has a mutually supportive relationship with Emticia, Sphingobium, Bacillus, Haliscomenobacter and Reyranella. Polaribacter has a mutually reinforcing relationship with Marinomonas and Bizionia and Polaribacter, whereas Hepatoplasma has a suppressive effect. Psychrilyobacter also has a mutually reinforcing relationship with Alteromonas, Shewanella, WH1_8. Mesoflavibacter has a mutually promoting relationship with Phaeobacter, Colwellia, Bacillus, Psychrobacter and Cohaesibacter.

3.5 Statistical analysis of metabolites

Percentage content of 20 metabolites in the gut of *C. japonica*: Glycine in AH (0.069%), CK (0.075); Galactose in AH (0.073%), CK (0.63%); Proline in AH (0.068%), CK (0.063%); Tyrosine in AH (0.063%), CK (0.059%). Leucine in AH (0.059%), CK (0.059%); Phosphoric acid in AH (0.053%), CK (0.058%); Glucose in AH (0.061%), CK (0.050%) (Figure 4A). These findings demonstrate that there is still a direct difference between AH and CK. PLS-DA looks for factors that can find the maximum distinction between sample groupings (a factor can be interpreted as a weighted sum of all metabolites). Discriminant analysis encodes the discontinuous

categorical variable to be predicted as a latent variable, which is continuous, so that a regression can be created between the explanatory and latent variables and solved using the theory of least squares regression. PLS-DA finds a linear regression model by projecting the predictor and observed variables separately into a new space (the dimensions of the new space are independent of each other and there is no covariance problem). In Figure 4B, each point corresponds to a sample and the PLS-DA effect plot is the value of the two factors that discriminate the best. The AH samples were found to be concentrated on the left side of the PLS-DA effect plot and CK on the right side of the PLS-DA effect plot.

3.6 Metabolic pathway analysis

The degree of reduction in the predictive accuracy of the random forest by making the value of a metabolite a random number is the "Mean Decrease Accuracy". Among the 15 most important metabolites, glucose, 9-Z-octadecenoic acid, 4-hydroxyproline and 1-monohexadecanoylglycerol increased the most in *C. japonica* infected with *A. hydrophila* (Figure 4C). The levels of xylitol, ornithine and uracil were decreased in *C. japonica* infected with *A. hydrophila*. The metabolic pathways that were significantly enriched in differential metabolites are shown in Figure 5A. Metabolites that increased in the gut of *C. japonica* after infection with *A. hydrophila* were associated with beta-alanine metabolism, nitrogen metabolism, inositol phosphate metabolism, galactose metabolism, histidine metabolism, ascorbate and aldarate metabolism, fatty acid biosynthesis, aminoacyl-tRNA biosynthesis and arginine and proline metabolism.

As can be seen in Figure 5C, alanine, beta-alanine, carnosine and L-histidine levels were increased.

3.7. 16S rRNA and metabolite association analysis

Polaribacter showed a positive correlation with pyruvic acid, myo-inosit-1-phosphate, beta-alanine , glutamic acid, histidine, galactose and galactonic acid. Mesoflavibacter showed a positive correlation with pyruvic acid , myo-inosit-1-phosphate , beta-alanine , glutamic acid, histidine and alanine. Psychrilyobacter showed positive correlations with alanine, myo-inositol, glycerol-3-phosphate, arginine and malic acid. Fusibacter showed a positive correlation with alanine, myo-inositol, glycerol-3-phosphate, arginine and malic acid. Rhodobacter showed positive correlations with malic acid , Glutamine and histidine (Figure 5B). Photobacterium showed positive correlations with beta-alanine, alanine and histidine. Phormidium also showed positive correlations with beta-alanine, alanine and glutamine. The activity of metabolite related enzymes such as lipid peroxides, SOD, i-NOS, GST, GSH, LPO, GPX and POX showed a downward trend as shown in Figure 8. The activity of THL, HK and PK enzymes was upregulated. The level of NO also showed a downward trend (Figure 6).

4. Discussion

The relative abundance of some beneficial intestinal genera including Photobacterium, Rhodobacter, Polaribacter, Mesoflavibacter, Fusibacter and Phormidium was

331 increased in *C. japonica* after infection with *A. hydrophila*. *Litopenaeus vannamei* had
332 a significantly higher abundance of gut Photobacterium after infection with white spot
333 syndrome virus (WSSV), which inhibits the composition and function of the gut
334 microbiota in vivo and prevents WSSV infection (13). Research over the years has
335 found that the most predominant species in healthy fish is Rhodobacter, and that co-
336 culture with Roseobacter isolates and *Vibrio anguillarum* in artificial seawater-based
337 phytoplankton media reduces the viability of *Vibrio anguillarum* by approximately
338 10-fold or more (14). Cultivation of Phaeobacter and Vibrio together under different
339 growth conditions antagonised Vibrio *anguillarum*, reducing the number (15).
340 Alkaloids also increased probiotic Rhodobacter during immunostimulatory and
341 disease resistance in fish (16). Some bacteria in Polaribacter can degrade algal
342 polysaccharides (17). Phormidium produces lipids such as monogalactose
343 diacylglycerol and digalactose diacylglycerol, which are anti-inflammatory and
344 antibacterial active substances (18). The enrichment of Mesoflavibacter in the gut of
345 American white shrimp fed resistant starch may be involved in the degradation of
346 toxins and the production of beneficial metabolites, and a significant elevation of
347 Mesoflavibacter could prevent the reduction of potential pathogens (Formosa and
348 Pseudoalteromonas) (19). The key bacterial members associated with overweight
349 shrimps were mainly from Firmicutes (short bacilli and Fusibacter), both of which
350 were found to be in higher abundance than those with less weight. Fusibacter in
351 Firmicutes has been identified as a potential probiotic and antimicrobial peptide
352 producer (20) in sea bass. From the above findings, it is evident that these increased

353 probiotic abundances can suppress *A. hydrophila* through numerical dominance, with
354 mechanisms that include an anti-pathogenic chemical similar to an interferon protein
355 molecule that can be induced by bacterial molecules to be released by immune
356 cells(21). Presumably, this mechanism can interfere with the population sensing of *A.*
357 *hydrophila* in *C. japonica* pathogens through signal hijacking.
358
359 Increased metabolites in the gut of *C. japonica* after infection with *A. hydrophila*
360 include beta-alanine metabolism, nitrogen metabolism, inositol phosphate metabolism,
361 galactose metabolism, histidine metabolism, ascorbate and aldarate metabolism, fatty
362 acid biosynthesis, aminoacyl-tRNA biosynthesis, arginine and proline metabolism
363 (Figure 9). In this experiment, the metabolites of nitrogen and histidine were more
364 abundant in the gut of *C. japonica* after being infected with *A. hydrophila*. Nitrogen is
365 a key element in biological systems; it is a fundamental component of amino acids,
366 proteins and nucleic acids. Most amino acids are broken down in the liver, while some
367 can be broken down in the intestine(22). In hepatocytes, several amino acids can be
368 degraded by specific histidases and NH_3 is released in the cytosol (23). Aquatic
369 animals excrete 50% of their nitrogenous waste as ammonia (24). Certain amino acids
370 can be converted to glutamate; they include arginine, glutamine, histidine and proline.
371 Glutamate is transaminated by alanine transaminase, which catalyses the reaction of
372 glutamate with pyruvate to form alpha-ketoglutarate and alanine without releasing
373 ammonia (25). The alpha-ketoglutarate produced can be directed into the tricarboxylic
374 acid cycle and partially catabolised to malic acid. Malic acid can be directed out of the

375 tricarboxylic acid cycle by malic enzymes and converted to pyruvate. This would
376 provide a continuous supply of pyruvate to sustain the transamine reaction catalysed
377 by alanine transaminase to form α-ketoglutarate and alanine (26). According to this
378 theory, the metabolites of arginine, histidine and proline in the gut of *C. japonica* after
379 infection with *A. hydrophila* are less than those of alanine. In this experiment, GPX,
380 GST and GSH of the glutamate metabolic pathway were measured, and GST and
381 GSH activities were found to be lower than in normal *C. japonica*, while GPX was
382 not significantly changed. The activity of these enzymes showed that the glutamate
383 metabolites were relatively low, inhibiting their redox reactions, and that the excess
384 glutamate may have been involved in the pyruvate reaction to produce α-ketoglutarate
385 and alanine. Metabolites in the gut of *C. japonica* infected with *A. hydrophila* are
386 most abundant in alanine metabolites, which have two isomers, α-alanine and β-
387 alanine. Alanine metabolites are the most important metabolites in the gut of *C.*
388 *japonica* infected with *A. hydrophila*.
389
390 Myostatin is a dipeptide that is found in high concentrations in skeletal muscle. It is
391 synthesised by the amino acids L-histidine and β-alanine, catalysed by myostatin
392 synthase. In this experiment, we found that THL, HK and PK enzyme activities were
393 upregulated in *C. japonica* after infection with *A. hydrophila*. Myostatin readily
394 glycosylates with aldose and ketose, inhibits dihydroxyacetone glycosylation of
395 histidine and Lys residues, and resists glycosylation and cross-linking of ribose,
396 deoxyribose and fructose(27). The results of our study are quite close to those of

Hipkiss et al. In this experiment, we found that lipid peroxidation was reduced in *C. japonica* after infection with *A. hydrophila* and that increased β-alanine metabolites could potentially reduce the production of free radicals in skeletal muscle and reduce lipid peroxidation. It was found that the hepatopancreas NO content was reduced and nitric oxide synthase (i-NOS) activity was also reduced after infection with *A. hydrophila* and that this increased NH_3 content in nitrogen metabolism and water reduced blood cell counts and haemocyanin levels, inhibited blood cell phagocytosis, reduced SOD and phenoloxidase activity, and disrupted immune defence systems, including immune cells and immune response factors(28). Increased NH_3-N in water is reported to reduce the immunity of crabs to pathogens and their ability to scavenge free radicals(29). In the present experiment, *C. japonica* showed reduced activity of SOD and phenoloxidase in the hepatopancreas after infection with *A. hydrophila*.

The literature that has investigated the interaction between probiotics and pathogenic bacteria support the idea that probiotics inhibit pathogenic bacteria by competing for adhesion sites (30), aggregating with pathogenic bacteria and producing metabolites (31). However, the presence of conditionally pathogenic bacteria in the gut does not disappear with the presence of intestinal probiotics, suggesting that there may be interactions between probiotics and pathogenic bacteria other than antagonism(32). Therefore, we found that Mesoflavibacter, a representative of the intestinal probiotics of *C. japonica*, had a mutually promoting relationship with Phaeobacter, Colwellia, Bacillus, Psychrobacter and Cohaesibacter; Rhodobacter with Emticia, Sphingobium,

419 Bacillus, Haliscomenobacter and Reyranella; and Polaribacter with Marinomonas and
420 Bizionia (Figure 5). Kernbauer et al. (32) reported that some pathogens cause
421 diarrhoea and can promote enterocyte colonization, which helps to restore structural
422 and functional damage to the intestine caused by enteritis. As a typical conditional
423 pathogen, *L. monocytogenes* is present in the intestine of many healthy individuals
424 (33). To date, the biological significance of its presence has not been reported. This
425 suggests that conditional pathogenic bacteria in the gut of healthy crabs may also have
426 a symbiotic relationship with intestinal probiotics, promoting their growth and
427 multiplication and enhancing their prebiotic effect. This study verifies that
428 Phormidium interacts with Aeromonas and Azopira, and it can be inferred that
429 *Aeromonas hydrophila*, a pathogenic bacterium in *Aeromonas*, can also promote the
430 growth of other probiotics. It is hoped that more pathogens and probiotics will be
431 selected for further study to examine this stimulatory effect and molecular mechanism
432 and to explain this phenomenon more clearly.
433
434 Different tissues of animals, such as the skin, the hepatopancreas and the intestine,
435 contain a large number of bacteria. Due to improvements in 16s sequencing
436 technology, tens of millions of different microbial genes have been identified in the
437 human gut, thus exceeding the number of other animal genomes by a factor of several
438 hundred (34). This huge number of genes signifies that bacteria have a greater
439 metabolic function in their hosts, synthesising essential amino acids and potentially
440 participating in the metabolism of the host organism(35). As a result, the *C. japonica*

441 gut microbiome is considered to be a tissue with the metabolic potential to influence
442 the metabolism of *C. japonica*. This is because the gut microbiome allows the
443 nutrients contained in food to be processed and allows their components to be
444 adsorbed and reused by crab cells. Thanks to improved methods of metabolite
445 (metabolomics) analysis, recent analyses have shown that many of these metabolites
446 originate from the metabolism of intestinal bacteria. Classes such as Mesoflavibacter
447 showed positive correlations with pyruvic acid, myo-inosit-1-phosphate, beta-alanine,
448 glutamic acid, histidine and alanine; Fusibacter showed positive correlations with
449 alanine, myo-inositol, glycerol-3-phosphate, arginine and malic acid; Rhodobacter
450 showed a positive correlation with malic acid, glutamine and histidine;
451 Photobacterium showed a positive correlation with beta-alanine, alanine and histidine;
452 Phormidium showed a positive correlation with beta-alanine, alanine and glutamine.
453 This suggests that metabolites increased with the abundance of bacteria and therefore
454 showed a positive correlation. It is possible that the autoimmune system and the entry
455 of *A. hydrophila* into the intestinal tissues of *C. japonica* react immunologically and
456 that the organism is producing certain metabolites which may be metabolised by
457 various bacteria and absorbed into the circulation. In addition, some of these
458 metabolites are modified or bound in the liver to produce microbiota-host co-
459 metabolites(35). These microbial metabolites or co-metabolites can resist invasion by
460 *A. hydrophila*. For example, through specific receptors such as short-chain fatty acids,
461 indoles or myostatin, as described previously(36).
462

5. Conclusion

In conclusion, the results of this study suggest that some beneficial genera of bacteria in the intestine of *C. japonica* can inhibit *A. hydrophila* after infection. The most abundant metabolites in the gut of *C. japonica* infected with *A. hydrophila* were alanine metabolites. In this experiment, lipid, peroxide, SOD, i-NOS, phenol oxidase, GST and GSH and NO levels were found to be decreased in *C. japonica* infected with *A. hydrophila* in the intestine. The enzymatic activity of THL, HK and PK was upregulated in *A. hydrophila*-infected *C. japonica*. The probiotics in the intestinal tract of *C. japonica* have a mutually reinforcing relationship, promoting their growth and reproduction and enhancing their prebiotic effect. *C. japonica* metabolites showed a positive correlation with probiotic flora, suggesting that metabolites increased with the abundance of bacteria and that microbial metabolites or co-metabolites could resist invasion by *A. hydrophila*. The above results may contribute to further studies investigating the resistance of the crab to invading pathogenic bacteria. They also provide information for future research on relevant probiotic and metabolite pathways.

6. Acknowledgements

The authors would like to thank for Mengling Sun her help of sampling. This work was supported by National Key R&D Program of China (2020YFD0900305) Science Foundation of Jiangsu (NO. BK20191488) in China, Major project of hydrobios resources in Jiangsu province (ZYHB16-3) and agricultural major new variety creation project in Jiangsu province (PZCZ201743).

Reference

1. **Sudo H, Kajihara N, Fujii T.** 2008. Predation by the swimming crab Charybdis japonica and piscivorous fishes: a major mortality factor in hatchery-reared juvenile Japanese flounder Paralichthys olivaceus released in Mano Bay, Sado Island, Japan. Fisheries Research **89:**49-56.

2. **Zhao C, Ji N, Zhang B, Sun P, Feng W, Wei J, Chang Y.** 2014. Effects of covering behavior and exposure to a predatory crab Charybdis japonica on survival and HSP70 expression of juvenile sea urchins Strongylocentrotus intermedius. PloS one **9:**e97840.

3. **Xu XY, Shen YB, Fu JJ, Liu F, Guo SZ, Yang XM, Li JL.** 2012. Matrix metalloproteinase 2 of grass carp Ctenopharyngodon idella (CiMMP2) is involved in the immune response against bacterial infection. Fish & Shellfish Immunology **33**.

4. **Burr G, Gatlin D, Ricke S.** 2010. Microbial Ecology of the Gastrointestinal Tract of Fish and the Potential Application of Prebiotics and Probiotics in Finfish Aquaculture. Journal of the World Aquaculture Society **36**.

5. **Yuan YL, Xiao AX, Wu QY, Wen HL, You SL.** 2008. Infection with Hematodinium sp. in mud crabs Scylla serrata cultured in low salinity water in southern China. Diseases of Aquatic Organisms **82:**145-150.

6. **Givens CE, Burnett KG, Burnett LE, Hollibaugh JT.** 2013. Microbial communities of the carapace, gut, and hemolymph of the Atlantic blue crab, Callinectes sapidus. Marine biology **160:**2841-2851.

507 7. **Jagadeesan B, Gerner-Smidt P, Allard MW, Leuillet S, Winkler A, Xiao Y, Chaffron S,**
508 **Van Der Vossen J, Tang S, Katase M.** 2019. The use of next generation sequencing
509 for improving food safety: translation into practice. Food microbiology **79:**96-115.
510 8. **Liu H, Wang L, Liu M, Wang B, Jiang K, Ma S, Li Q.** 2011. The intestinal microbial
511 diversity in Chinese shrimp (Fenneropenaeus chinensis) as determined by PCR–
512 DGGE and clone library analyses. Aquaculture **317:**32-36.
513 9. **Li S, Sun L, Wu H, Hu Z, Liu W, Li Y, Wen X.** 2012. The intestinal microbial diversity
514 in mud crab (S cylla paramamosain) as determined by PCR-DGGE and clone library
515 analysis. Journal of applied microbiology **113:**1341-1351.
516 10. **Wu H-J, Sun L-B, Li C-B, Li Z-Z, Zhang Z, Wen X-B, Hu Z, Zhang Y-L, Li S-K.** 2014.
517 Enhancement of the immune response and protection against Vibrio
518 parahaemolyticus by indigenous probiotic Bacillus strains in mud crab (Scylla
519 paramamosain). Fish & shellfish immunology **41:**156-162.
520 11. **Lankadurai BP, Nagato EG, Simpson MJ.** 2013. Environmental metabolomics: an
521 emerging approach to study organism responses to environmental stressors.
522 Environmental Reviews **21:**180-205.
523 12. **Gago-Tinoco A, González-Domínguez R, García-Barrera T, Blasco-Moreno J,**
524 **Bebianno MJ, Gómez-Ariza J-L.** 2014. Metabolic signatures associated with
525 environmental pollution by metals in Doñana National Park using P. clarkii as
526 bioindicator. Environmental Science and Pollution Research **21:**13315-13323.
527 13. **Wang J, Huang Y, Xu K, Zhang X, Sun H, Fan L, Yan M.** 2019. White spot syndrome
528 virus (WSSV) infection impacts intestinal microbiota composition and function in

529 Litopenaeus vannamei. Fish & shellfish immunology **84:**130-137.

530 14. **Sharifah EN, Eguchi M.** 2011. The phytoplankton Nannochloropsis oculata enhances
531 the ability of Roseobacter clade bacteria to inhibit the growth of fish pathogen Vibrio
532 anguillarum. PLoS One **6:**e26756.

533 15. **Porsby CH, Nielsen KF, Gram L.** 2008. Phaeobacter and Ruegeria species of the
534 Roseobacter clade colonize separate niches in a Danish turbot (Scophthalmus
535 maximus)-rearing farm and antagonize Vibrio anguillarum under different growth
536 conditions. Applied and environmental microbiology **74:**7356-7364.

537 16. **She R, Li T-T, Luo D, Li J-B, Yin L-Y, Li H, Liu Y-M, Li X-Z, Yan Q-g.** 2017. Changes
538 in the intestinal microbiota of gibel carp (Carassius gibelio) associated with cyprinid
539 herpesvirus 2 (CyHV-2) infection. Current microbiology **74:**1130-1136.

540 17. **Nedashkovskaya OI, Kim S-G, Balabanova LA, Zhukova NV, Bakunina IY, Mikhailov**
541 **VV.** 2018. Polaribacter staleyi sp. nov., a polysaccharide-degrading marine bacterium
542 isolated from the red alga Ahnfeltia tobuchiensis. International journal of systematic
543 and evolutionary microbiology **68:**623-629.

544 18. **Belhaj D, Frikha D, Athmouni K, Jerbi B, Ahmed MB, Bouallagui Z, Kallel M, Maalej S,**
545 **Zhou J, Ayadi H.** 2017. Box-Behnken design for extraction optimization of crude
546 polysaccharides from Tunisian Phormidium versicolor cyanobacteria (NCC 466):
547 partial characterization, in vitro antioxidant and antimicrobial activities. International
548 journal of biological macromolecules **105:**1501-1510.

549 19. **Duan Y, Wang Y, Liu Q, Dong H, Li H, Xiong D, Zhang J.** 2019. Changes in the
550 intestine microbial, digestion and immunity of Litopenaeus vannamei in response to

551 dietary resistant starch. Scientific reports **9:**1-10.

552 20. **Yang X, Yousef AE.** 2018. Antimicrobial peptides produced by Brevibacillus spp.:
553 structure, classification and bioactivity: a mini review. World journal of microbiology
554 and biotechnology **34:**1-10.

555 21. **Drobysheva AV, Panafidina SA, Kolesnik MV, Klimuk EI, Sokolova ML.** 2020.
556 Structure and function of virion RNA polymerase of a crAss-like phage. Nature**:**1-4.

557 22. **Karlsson A, Eliason EJ, Mydland LT, Farrell AP, Kiessling A.** 2006. Postprandial
558 changes in plasma free amino acid levels obtained simultaneously from the hepatic
559 portal vein and the dorsal aorta in rainbow trout (Oncorhynchus mykiss). Journal of
560 Experimental Biology **209:**4885-4894.

561 23. **Youngson A, Cowey C, Walton M.** 1982. Some properties of serine pyruvate
562 aminotransferase purified from liver of rainbow trout Salmo gairdneri. Comparative
563 Biochemistry and Physiology Part B: Comparative Biochemistry **73:**393-398.

564 24. **Weihrauch D, Wilkie MP, Walsh PJ.** 2009. Ammonia and urea transporters in gills of
565 fish and aquatic crustaceans. Journal of experimental biology **212:**1716-1730.

566 25. **Ip YK, Lem C, Chew SF, Wilson JM, Randall DJ.** 2001. Partial amino acid catabolism
567 leading to the formation of alanine in Periophthalmodon schlosseri (mudskipper): a
568 strategy that facilitates the use of amino acids as an energy source during locomotory
569 activity on land. Journal of Experimental Biology **204:**1615-1624.

570 26. **Chew SF, Wong MY, Tam WL, Ip YK.** 2003. The snakehead Channa asiatica
571 accumulates alanine during aerial exposure, but is incapable of sustaining locomotory
572 activities on land through partial amino acid catabolism. Journal of experimental

biology **206:**693-704.

27. **Hipkiss AR, Brownson C, Carrier MJ.** 2001. Carnosine, the anti-ageing, anti-oxidant dipeptide, may react with protein carbonyl groups. Mechanisms of Ageing & Development **122:**1431-1445.

28. **Chen YY, Chen JC, Lin YC, Su-Tuen Y, Huang CL.** 2015. White Shrimp Litopenaeus vannamei That Have Received Gracilaria tenuistipitata Extract Show Early Recovery of Immune Parameters after Ammonia Stressing. Marine Drugs **13**.

29. **Chen YY, Sim SS, Chiew SL, Yeh ST, Liou CH, Chen JC.** 2012. Dietary administration of a Gracilaria tenuistipitata extract produces protective immunity of white shrimp Litopenaeus vannamei in response to ammonia stress. Aquaculture **370-371:**26-31.

30. **Salminen S, Nybom S, Meriluoto J, Collado MC, Vesterlund S, El-Nezami H.** 2010. Interaction of probiotics and pathogens—benefits to human health? Current opinion in biotechnology **21:**157-167.

31. **Gagnon M, Zihler A, Chassard C, Lacroix C.** 2011. Ecology of probiotics and enteric protection, p. 65-85, Probiotic Bacteria and Enteric Infections. Springer.

32. **Kernbauer E, Ding Y, Cadwell K.** 2014. An enteric virus can replace the beneficial function of commensal bacteria. Nature **516:**94-98.

33. **Adzitey F, Huda N.** 2010. Listeria monocytogenes in foods: incidences and possible control measures. African Journal of Microbiology Research **4:**2848-2855.

34. **Tierney BT, Yang Z, Luber JM, Beaudin M, Wibowo MC, Baek C, Mehlenbacher E, Patel CJ, Kostic AD.** 2019. The landscape of genetic content in the gut and oral

595 human microbiome. Cell host & microbe **26:**283-295. e288.

596 35. **Holmes E, Li J, Marchesi J, Nicholson J.** 2012. Gut Microbiota Composition and
597 Activity in Relation to Host Metabolic Phenotype and Disease Risk. Cell Metabolism
598 **16:**559-564.

599 36. **Rahim MA, Chilloux J, Martinez-Gili L, Neves AL, Myridakis A, Gooderham N, Dumas**
600 **ME.** 2019. Diet-induced metabolic changes of the human gut microbiome: importance
601 of short-chain fatty acids, methylamines and indoles. Acta Diabetologica.

602

603 Table 1 Statistical table of DADA2 denoising to generate (Operational Taxonomic
604 Units) OTUs.

sample-id	input	filtered	denoised	merged	non-chimeric
AH1	51820.0	46995.0	46995.0	46262.0	42540.0
AH2	53801.0	48149.0	48149.0	44588.0	27026.0
AH3	40419.0	37184.0	37184.0	34778.0	16628.0
AH4	48431.0	43146.0	43146.0	41123.0	33171.0
AH5	58952.0	53367.0	53367.0	49501.0	25823.0
AH6	49210.0	44315.0	44315.0	43513.0	40142.0
CK1	52331.0	47532.0	47532.0	43157.0	21781.0
CK2	48898.0	44245.0	44245.0	40835.0	22046.0
CK3	38808.0	34699.0	34699.0	33159.0	26160.0
CK4	43823.0	39674.0	39674.0	38840.0	27073.0
CK5	58821.0	53665.0	53665.0	50405.0	27483.0
CK6	32453.0	28733.0	28733.0	26260.0	14226.0

605

606 Figure 1: Workflow for the analysis of 16SRNA and metabolomic data in response to
607 berberine.

608

609 Figure 2: (A) Histogram of the relative distribution of each subgroup at the phylum
610 level (top 15 species in relative abundance), the vertical coordinate (sequence number
611 percent) indicates the ratio of the number of sequences annotated to that phylum level
612 to the total annotated data, the top-down colour order of the histogram corresponds to
613 the colour order of the legend on the right. *C. japonica* injected with 10^5 CFU/L of *A.*
614 *hydrophila* (AH) and control (CK). (B) Venn diagram of shared or endemic species
615 (when the number of subgroups is less than or equal to 5). (C) Box plot of Shannon's
616 index for *C. japonica* injected with 10^5 CFU/L of *A. hydrophila* (AH) and control
617 (CK).
618
619 Figure 3: (A) Heat map of the phylogenetic evolutionary tree and the distribution of
620 abundance between groups. The evolutionary tree is shown on the left, the different
621 coloured branches represent different clades and each end branch represents an OTU.
622 The end annotates the genus classification to which the corresponding OTU belongs.
623 The heat map on the right is the normalised abundance. The mean of the abundance is
624 0 and the standard deviation is 0.5. Twelve samples were divided into two groups: AH
625 and CK. (B) Species interaction network at the taxonomic level. Circles represent a
626 species, the size represents its relative abundance, different colours represent different
627 species phylum classifications, lines between circles represent a significant correlation
628 between these two species (p-value less than 0.05). Red lines indicate positive
629 correlations, blue lines indicate negative correlations. The thicker the line, the larger
630 the absolute value of the correlation coefficient.

631

632 Figure 4: (A) Histogram of the top 20 metabolites. *C. japonica* injected with 10^5
633 CFU/L of *A. hydrophila* (AH) and control (CK). (B) PLS-DA point cloud, *C. japonica*
634 injected with 10^5 CFU/L of *A. hydrophila* (AH) and control (CK). (C) The top 15
635 metabolites in the random forest. The horizontal coordinate on the left panel is "Mean
636 Decrease Accuracy"; the right panel is a heat map of the levels of the 15 metabolites
637 in the two subgroups. *C. japonica* injected with 10^5 CFU/L of *A. hydrophila* (AH) and
638 the control group (CK).

639

640 Figure 5: (A) RA enrichment analysis, the horizontal coordinate is the enrichment
641 multiplier, which is the number of observed metabolites/theoretical metabolites in the
642 metabolic pathway. The p-value magnitude is indicated by colour, the darker the
643 colour, the smaller the p-value. (B) Association analysis results in the horizontal axis
644 are metabolites, vertical axis are genus. Colours represent the r value, red indicates
645 positive correlation, blue indicates negative correlation. The darker the colour the
646 stronger the correlation; asterisks indicate that the p-value of the correlation is less
647 than or equal to 2.50. (C) Metabolites and metabolic pathways in *C. japonica*
648 (Acipenser japonicus) after infection with *A. hydrophila*. The red metabolites are
649 those that differed significantly between subgroups

650

651 Figure 6: Relevant enzymes in hepatopancreas tissue of *C. japonica* treated with *A.*
652 *hydrophila*. AH, the experimental group; CK, the control group. *Significantly (P <

653 0.05) different from control values.

654

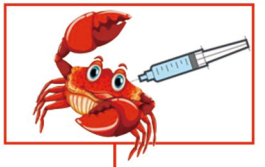

Aeromonas hydrophila
10^5 (CFU)/L

DNA extraction and detection → PCR amplification → Product purification

High throughput sequencing → Miseq machine sequencing → Library preparation and library inspection

Sample discount → Representative sequence (feature /OTU

experimental flow of 16S rRNA

experimental flow of metabolome

Data acquisition ← Mass spectrometry detection ← Metabolite extraction

Peak extraction screening → Compound identification Set → Shengxin analysis

Data standardization ← Batch correction ← Data QC quality control

Species annotation

①. Species annotation statistics

②. Analysis of differences between groups

Correlation analysis

①. Species interraction network analysis

Phylogenetic relationship

①. Evolution diagram of dominant species

Related metabolite enzyme activity

Basic statistics and visualization of metabolite content

①. Column diagram

②. PCA

Advanced analysis

①. Enrichment analysis

②. Metabolic pathway map

Characteristic metabolite screening

①. Basic discriminant analysis

②. Random forest

Alpha direrisify

①. Alpha direrisity index

Graph of correlation analysis results

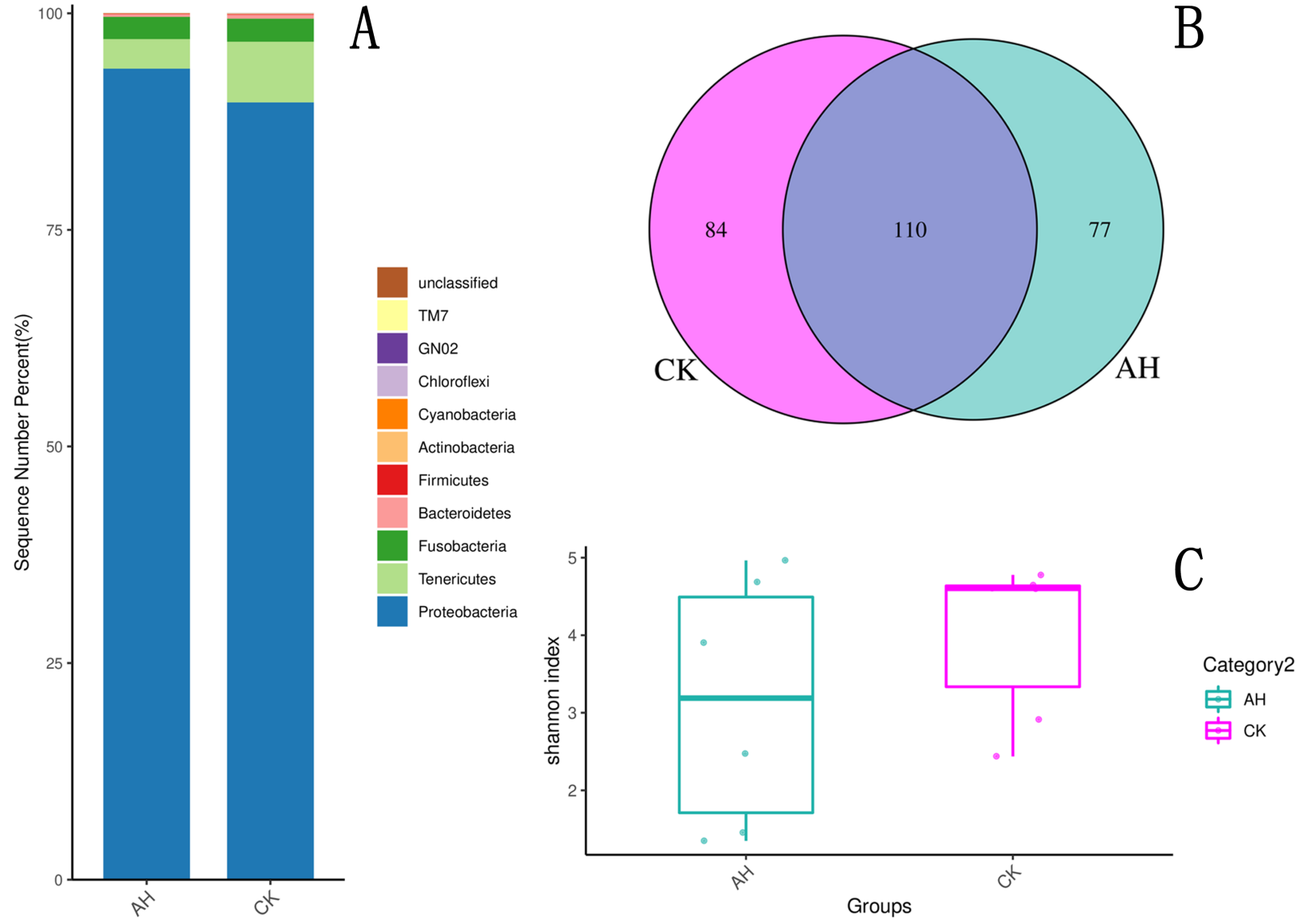
A
100
75
50
25
0
Sequence Number Percent(%)
AH
CK
unclassified
TM7
GN02
Chloroflexi
Cyanobacteria
Actinobacteria
Firmicutes
Bacteroidetes
Fusobacteria
Tenericutes
Proteobacteria
B
84
110
77
CK
AH
C
shannon index
5
4
3
2
AH
CK
Groups
Category2
AH
CK

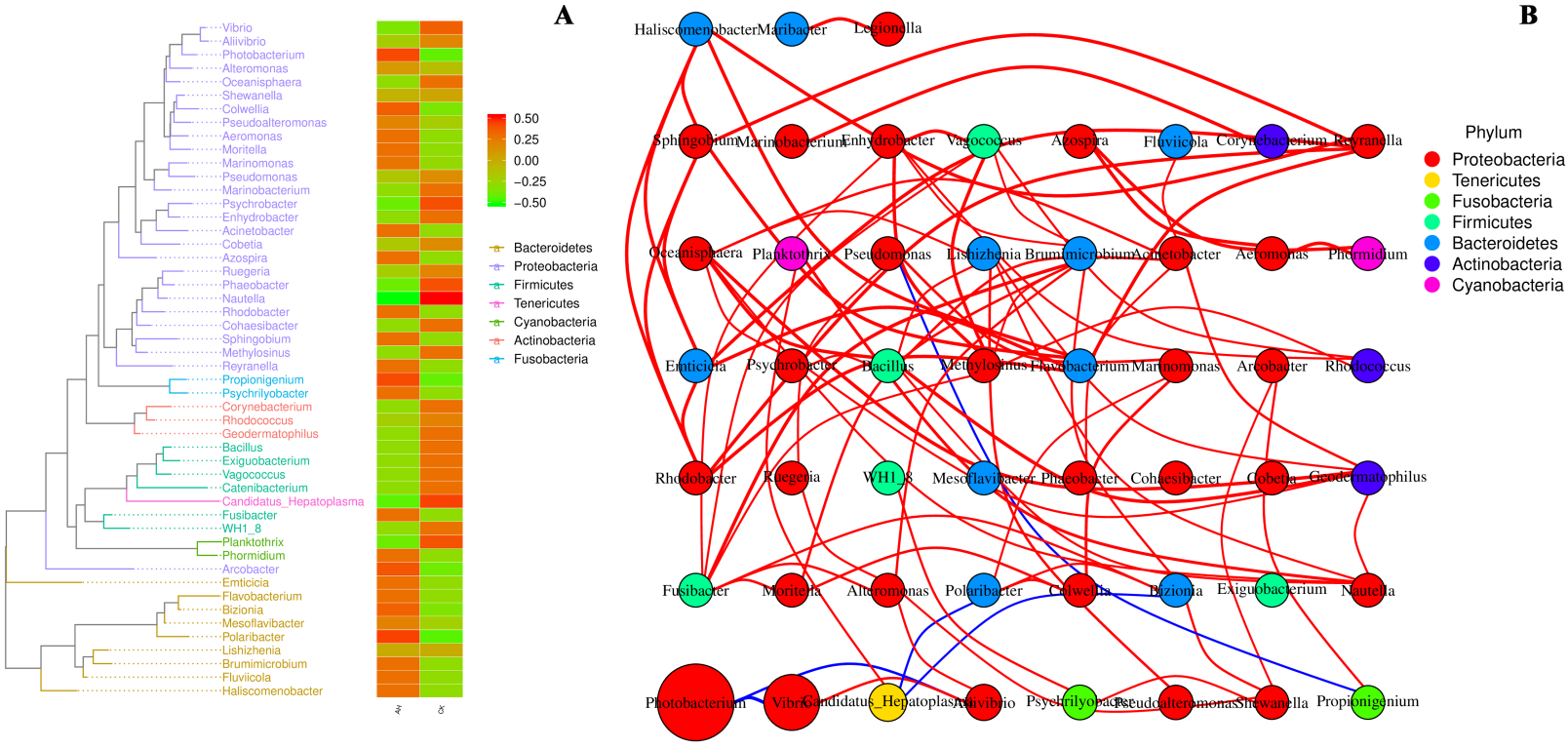
A
Vibrio
Aliivibrio
Photobacterium
Alteromonas
Oceanisphaera
Shewanella
Colwellia
Pseudoalteromonas
Aeromonas
Moritella
Marinomonas
Pseudomonas
Marinobacterium
Psychrobacter
Enhydrobacter
Acinetobacter
Cobetia
Azospira
Ruegeria
Phaeobacter
Nautella
Rhodobacter
Cohaesibacter
Sphingobium
Methylosinus
Reyranella
Propionigenium
Psychrilyobacter
Corynebacterium
Rhodococcus
Geodermatophilus
Bacillus
Exiguobacterium
Vagococcus
Catenibacterium
Candidatus_Hepatoplasma
Fusibacter
WH1_8
Planktothrix
Phormidium
Arcobacter
Emticicia
Flavobacterium
Bizionia
Mesoflavibacter
Polaribacter
Lishizhenia
Brumimicrobium
Fluviicola
Haliscomenobacter
0.50
0.25
0.00
−0.25
−0.50
Bacteroidetes
Proteobacteria
Firmicutes
Tenericutes
Cyanobacteria
Actinobacteria
Fusobacteria
Hy
Or
B
Haliscomenobacter
Maribacter
Legionella
Sphingobium
Marinobacterium
Enhydrobacter
Vagococcus
Azospira
Fluviicola
Corynebacterium
Reyranella
Oceanisphaera
Planktothrix
Pseudomonas
Lishizhenia
Brumimicrobium
Acinetobacter
Aeromonas
Phormidium
Emticicia
Psychrobacter
Bacillus
Methylosinus
Flavobacterium
Marinomonas
Arcobacter
Rhodococcus
Rhodobacter
Ruegeria
WH1_8
Mesoflavibacter
Phaeobacter
Cohaesibacter
Cobetia
Geodermatophilus
Fusibacter
Moritella
Alteromonas
Polaribacter
Colwellia
Bizionia
Exiguobacterium
Nautella
Photobacterium
Vibrio
Candidatus_Hepatoplasma
Aliivibrio
Psychrilyobacter
Pseudoalteromonas
Shewanella
Propionigenium
Phylum
Proteobacteria
Tenericutes
Fusobacteria
Firmicutes
Bacteroidetes
Actinobacteria
Cyanobacteria

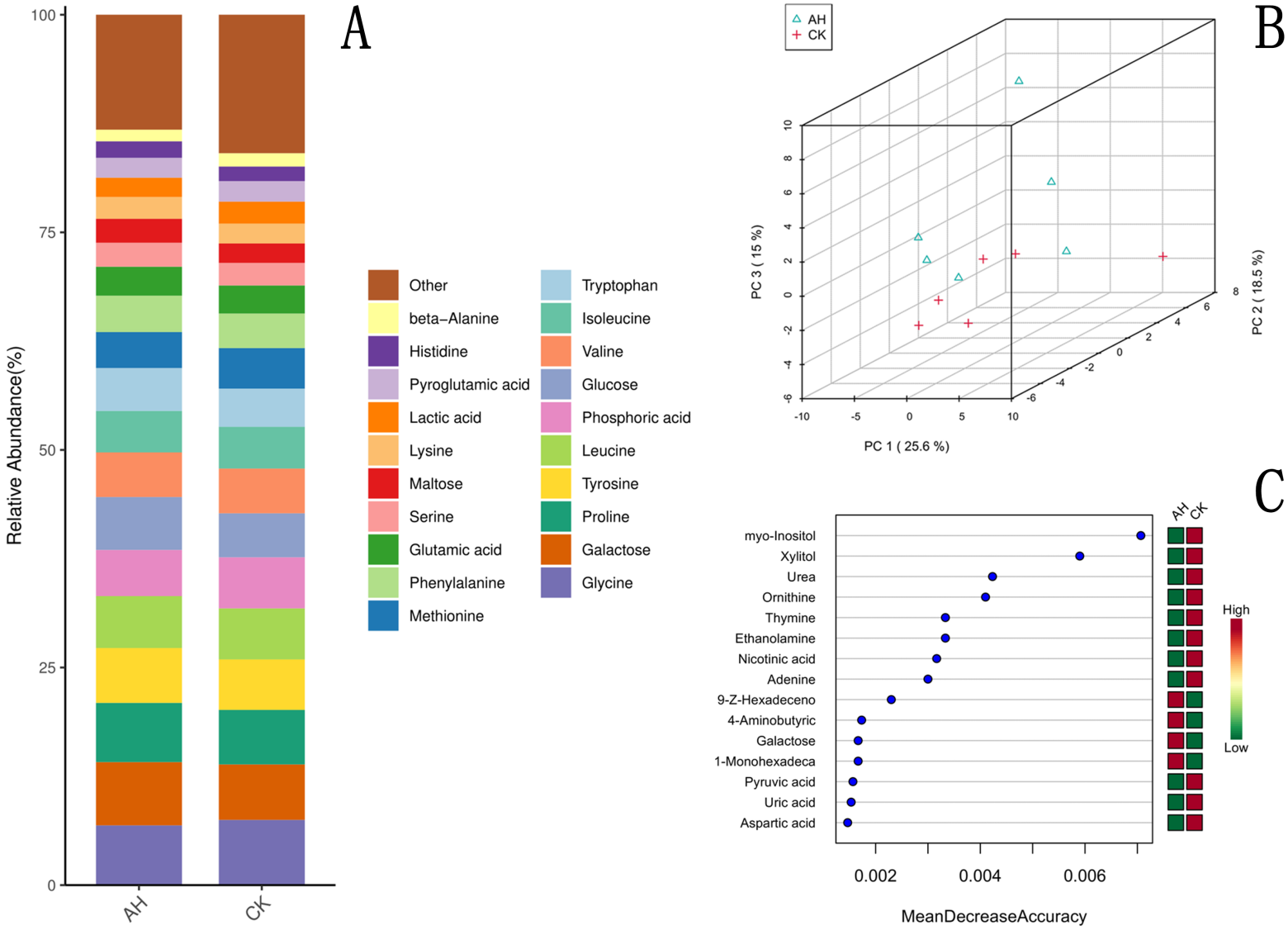
A
100
75
50
25
0
Relative Abundance(%)
AH
CK
Other
beta−Alanine
Histidine
Pyroglutamic acid
Lactic acid
Lysine
Maltose
Serine
Glutamic acid
Phenylalanine
Methionine
Tryptophan
Isoleucine
Valine
Glucose
Phosphoric acid
Leucine
Tyrosine
Proline
Galactose
Glycine
B
AH
CK
PC 3 (15 %)
PC 1 (25.6 %)
PC 2 (18.5 %)
C
myo-Inositol
Xylitol
Urea
Ornithine
Thymine
Ethanolamine
Nicotinic acid
Adenine
9-Z-Hexadeceno
4-Aminobutyric
Galactose
1-Monohexadeca
Pyruvic acid
Uric acid
Aspartic acid
0.002
0.004
0.006
MeanDecreaseAccuracy
High
Low

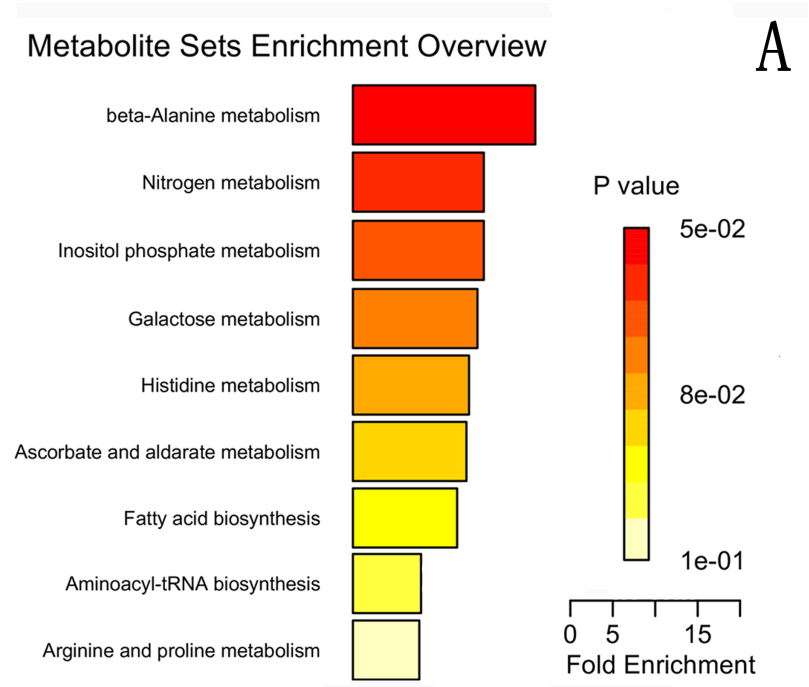
Metabolite Sets Enrichment Overview
A
beta-Alanine metabolism
Nitrogen metabolism
Inositol phosphate metabolism
Galactose metabolism
Histidine metabolism
Ascorbate and aldarate metabolism
Fatty acid biosynthesis
Aminoacyl-tRNA biosynthesis
Arginine and proline metabolism
P value
5e-02
8e-02
1e-01
0 5 15
Fold Enrichment

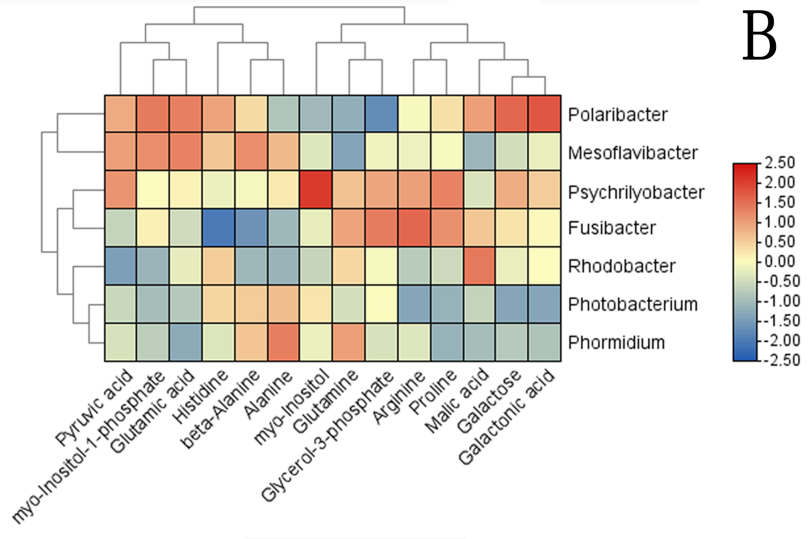
B
Polaribacter
Mesoflavibacter
Psychrilyobacter
Fusibacter
Rhodobacter
Photobacterium
Phormidium
2.50
2.00
1.50
1.00
0.50
0.00
-0.50
-1.00
-1.50
-2.00
-2.50
Pyruvic acid
myo-Inositol-1-phosphate
Glutamic acid
Histidine
beta-Alanine
Alanine
myo-Inositol
Glutamine
Glycerol-3-phosphate
Arginine
Proline
Malic acid
Galactose
Galactonic acid

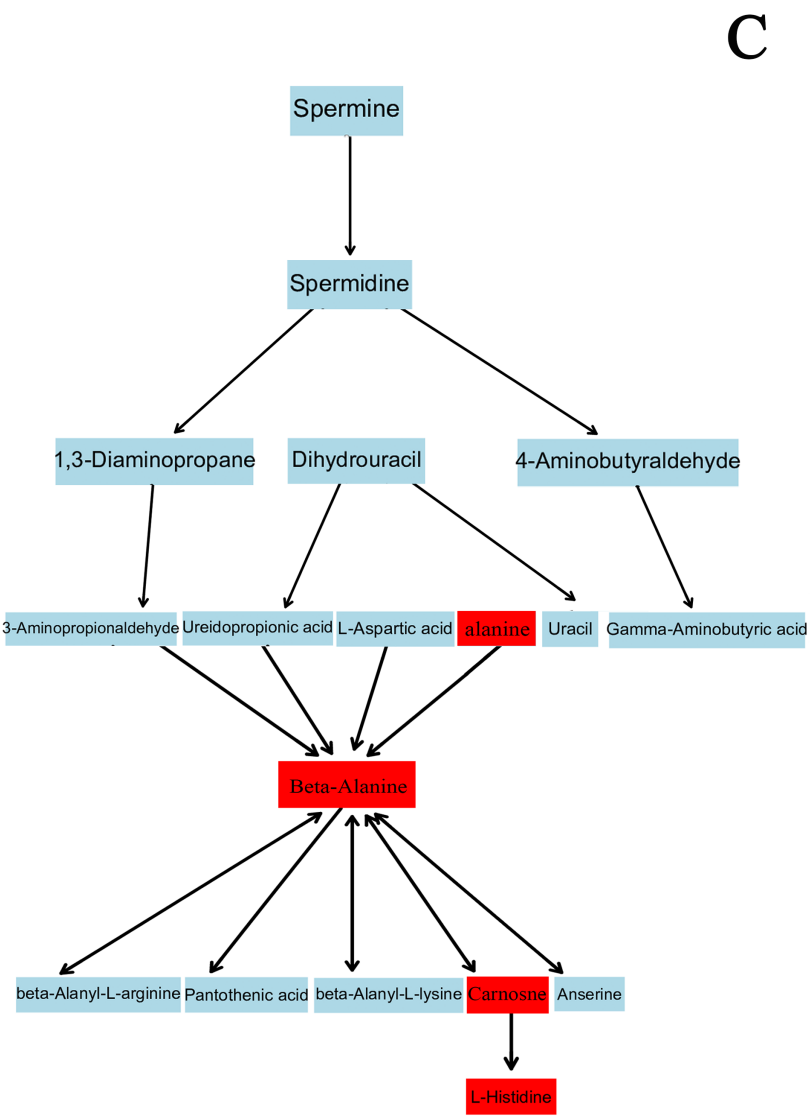
C
Spermine
Spermidine
1,3-Diaminopropane
Dihydrouracil
4-Aminobutyraldehyde
3-Aminopropionaldehyde
Ureidopropionic acid
L-Aspartic acid
alanine
Uracil
Gamma-Aminobutyric acid
Beta-Alanine
beta-Alanyl-L-arginine
Pantothenic acid
beta-Alanyl-L-lysine
Carnosne
Anserine
L-Histidine

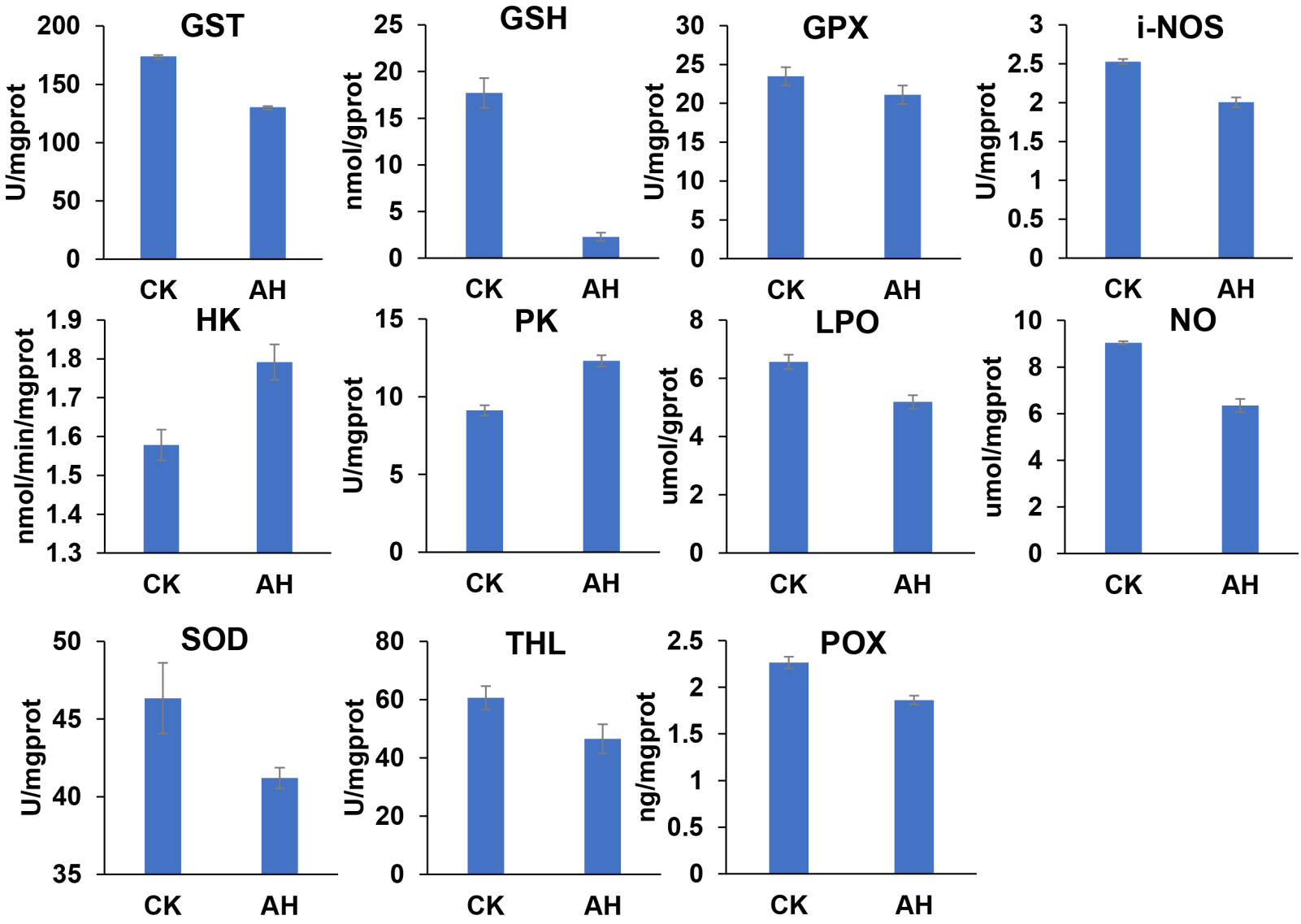
GST
U/mgprot
200
150
100
50
0
CK
AH
GSH
nmol/gprot
25
20
15
10
5
0
CK
AH
GPX
U/mgprot
30
25
20
15
10
5
0
CK
AH
i-NOS
U/mgprot
3
2.5
2
1.5
1
0.5
0
CK
AH
HK
nmol/min/mgprot
1.9
1.8
1.7
1.6
1.5
1.4
1.3
CK
AH
PK
U/mgprot
15
10
5
0
CK
AH
LPO
umol/gprot
8
6
4
2
0
CK
AH
NO
umol/mgprot
10
8
6
4
2
0
CK
AH
SOD
U/mgprot
50
45
40
35
CK
AH
THL
U/mgprot
80
60
40
20
0
CK
AH
POX
ng/mgprot
2.5
2
1.5
1
0.5
0
CK
AH